PERGAMON

J. Mech. Phys. Solids 47 (1999) 2235–2272

JOURNAL OF THE MECHANICS AND PHYSICS OF SOLIDS

Effect of imperfections on the yielding of two-dimensional foams

C. Chen, T.J. Lu, N.A. Fleck*

Department of Engineering, University of Cambridge, Trumpington Street, Cambridge, CB2 1PZ, UK

Received 29 October 1998; received in revised form 2 April 1999

Abstract

The influence of each of the six different types of morphological imperfection—waviness, non-uniform cell wall thickness, cell-size variations, fractured cell walls, cell-wall misalignments, and missing cells—on the yielding of 2D cellular solids has been studied systematically for biaxial loading. Emphasis is placed on quantifying the knock-down effect of these defects on the hydrostatic yield strength and upon understanding the associated deformation mechanisms. The simulations in the present study indicate that the high hydrostatic strength, characteristic of ideal honeycombs, is reduced to a level comparable with the deviatoric strength by several types of defect. The common source of this large knock-down is a switch in deformation mode from cell wall stretching to cell wall bending under hydrostatic loading. Fractured cell edges produce the largest knock-down effect on the yield strength of 2D foams, followed in order by missing cells, wavy cell edges, cell edge misalignments, Γ Voronoi cells, δ Voronoi cells, and non-uniform wall thickness. A simple elliptical yield function with two adjustable material parameters successfully fits the numerically predicted yield surfaces for the imperfect 2D foams, and shows potential as a phenomenological constitutive law to guide the design of structural components made from metallic foams.

Keywords: A. Microstructures; B. Elastic-plastic material; Foam material; C. Finite elements

* Corresponding author. Tel.: +44-01223-332650; fax: +44-01223-332662.
E-mail address: naf1@eng.cam.ac.uk (N.A. Fleck)

0022-5096/99/$ - see front matter
PII: S0022-5096(99)00030-7

1. Introduction

Low density metallic foams are a new class of engineering materials with promising mechanical, thermal, electrical and acoustical properties. A wide range of applications is currently under exploration, including lightweight components for vehicles, heat dissipation media for high power electronics, and sound absorbing devices for noise and vibration control. Experimentally validated micromechanical models of metallic foams are needed as a framework for structure-property relationships, and to aid design. The mechanical properties of cellular materials have been studied extensively, and can be found in several comprehensive surveys (Weaire and Fortes, 1994; Gibson and Ashby, 1997; Evans et al., 1998).

Idealised foams such as the hexagonal honeycomb possess a high ratio of hydrostatic strength to deviatoric strength: under hydrostatic loading their cell walls deform by stretching whereas under deviatoric loading they yield at lower stress levels by bending (Gibson and Ashby, 1997). Most commercially available metallic foams contain processing induced morphological defects which degrade their deviatoric strength by an order of magnitude (Sugimura et al., 1997; Evans et al., 1998), and their hydrostatic strength to a level comparable with their deviatoric strength (Deshpande and Fleck, 1998; Gioux et al., 1998). These include wavy cell walls, non-uniform wall thickness, cell wall misalignments, broken cell walls, missing cells, and a random dispersion of cell size. The extent to which each of these imperfections is responsible for the observed knock-down in hydrostatic yield strength is addressed in this paper for the simplified case of a 2D foam, using analytical and finite element techniques.

1.1. Processing defects in metallic foams

Metallic foams are most frequently made by foam casting or by directional solidification. For instance, a batch casting method is used by Shinko Wire to manufacture a closed cell aluminium alloy foam under the tradename of 'Alporas'. First, a small amount of calcium (Ca) is added to the molten aluminium alloy in a container to increase its viscosity. When the molten alloy has attained the desired viscosity, a foaming agent titanium hydride (TiH_2) is added; at the same time, the stirring speed is increased. The titanium hydride decomposes at 720°C to create hydrogen bubbles; a hydrogen over-pressure is applied to control the development of these bubbles. A sufficiently large viscosity is needed to prevent premature bubble coalescence. If the viscosity is too large, however, a rapid and uniform dispersion of the foaming agent in the melt becomes difficult, and the final porosity is low. The cellular structure of typical metallic foams exhibits several morphological imperfections, including curved and wrinkled cell walls, non-uniform wall thickness, non-uniform cell size distribution, fractured cell-walls, and missing cells.

Another type of aluminium alloy foam, under the tradename of 'Duocel', is manufactured by ERG by a directional solidification route and contains open

polyhedral cells. Metallographic studies reveal that the cellular structure of a typical ERG foam has a higher morphological quality than that of currently available closed cell foams (e.g. Alporas foam). The most likely morphological defect in an ERG foam is in the form of curved and wavy cell walls; here, Plateau's laws for minimal surface area do not apply as the processing of ERG and other metallic foams involves viscous forces in addition to surface tension (Kraynik et al., 1997).

An intriguing question arises as to whether the yield strength of a metallic foam having either closed or open cells is weakened by the presence of morphological imperfections and whether this involves a change of yielding mechanism from cell-wall stretching to cell-wall bending under hydrostatic loading. To gain some insight into this problem we shall consider the biaxial yield response of 2D metallic foams weakened by various morphological defects.

1.2. Survey of relevant literature and aim of study

An understanding of the yield behaviour of cellular metals is important for structural applications, yet the existing literature has largely focused on regular honeycombs. It is now well established that the in-plane hydrostatic strength of a perfect hexagonal honeycomb is governed by cell wall stretching and is proportional to the relative density $\bar{\rho}$, while its deviatoric strength is set by cell wall bending and scales with $\bar{\rho}^2$ (Gibson and Ashby, 1997). Thus, the yield surface is elongated along the hydrostatic axis in biaxial stress space. Using simple beam theory, Klintworth and Stronge (1988) proposed failure envelopes for regular honeycombs with respect to various elastic and plastic cell crushing modes; these are used together with the associated flow rule of plasticity to describe the in-plane indentation of a honeycomb by a plane punch (Klintworth and Stronge, 1989). Gibson et al. (1989) studied the biaxial yield surface of 2-dimensional honeycombs and the triaxial yield surface of 3-dimensional open-celled foams. These studies suggest that the plastic yield surface of regular honeycombs may be truncated by elastic buckling in compression and by brittle fracture in tension.

Several attempts have been made to account for the effects of morphological defects on the elastic and plastic properties of cellular solids. Warren and Kraynik (1987) and Kraynik et al. (1991) found that the presence of Plateau borders (non-uniform wall thickness) has only a small effect on the elastic response of honeycombs. Simone and Gibson (1998a) considered the effect of Plateau borders on the mechanical properties of hexagonal honeycombs and of idealised cellular foams with closed tetrakaidecahedral cells. Their finite element results suggest that the distribution of material in the cell walls has little effect upon the Young's modulus and has only a moderate influence upon the uniaxial yield strength. They argue that the maximum bending moments appear at the joints of the honeycomb and so the presence of Plateau borders has only a small effect on the Young's modulus. Grenestedt and Tanaka (1998) used the finite element method to study the influence of non-uniform cell wall thickness on the shear and bulk modulus of a flat-faced Kelvin structure, consisting of 14-sided closed cells in a BCC

arrangement. It was found that both moduli are rather insensitive to thickness variations, at fixed overall relative density.

The effects of cell face curvature and wiggles on the mechanical properties of regular honeycombs and of tetrakaidecahedral closed cell foams were studied by Simone and Gibson (1998b). They found that wavy imperfections can reduce significantly the Young's modulus and the uniaxial yield strength of the foam. Grenestedt (1998) has shown that wavy imperfections give a bigger reduction in the Voigt upper bound bulk modulus for open cell foams than for closed cell foams. He assumed affine deformation of the foams, and argued that cell wall waviness reduces the stretching stiffness of the beam-like cell walls in an open cell foam more than it reduces the stiffness of the shell-like cell walls in a closed cell foam. Grenestedt (1997) has also studied the effect of wavy imperfections on the yield behaviour of an open cell foam. In agreement with Gibson and Ashby (1997) he argued that the hydrostatic strength of the perfect foam is governed by cell wall stretching and scales with $\bar{\rho}$. For sufficiently large values of waviness, however, bending dominates the response and the strength scales with $\bar{\rho}^{3/2}$ under all stress states.

Silva et al. (1995) used a finite element method to model a 2D random Voronoi distribution of cells and found that 'the relations between microstructural and elastic properties for non-periodic honeycombs are, on average, not different from those for periodic honeycombs'. Silva and Gibson (1997) investigated the influence of random cellular microstructures and missing cell walls on the Young's modulus and uniaxial yield strength of 2D Voronoi honeycombs. They found that the uniaxial compressive yield strength of a Voronoi honeycomb is about 30% less than that of a perfect honeycomb at the same relative density level, and that defects, introduced by removing some of the cell walls at random locations, lead to a sharp decrease in the uniaxial stiffness and strength of both Voronoi and perfect honeycombs. Through a combination of analytical and finite element techniques Triantafyllidis and Schraad (1998) found that the yield surface of a perfect hexagonal honeycomb provides an upper bound for the yield surfaces of honeycombs with microstructural imperfections.

Kraynik et al. (1997) have presented a finite element study of the elastic response of a 3D random foam. They used Voronoi cells as the starting microstructures and then a surface evolution program to generate random soap froths of minimal surface energy. The cell walls are assumed to consist of linear elastic material but the overall response is found to be non-linear due to finite deformation effects. Under uniaxial compression, the stress-strain response of the foam is very similar to that of a regular foam with open Kelvin cells. However, under hydrostatic loading, the peak stress for a random Voronoi foam is much less than that for a perfect Kelvin foam. Kraynik et al. (1997) suggest that, under hydrostatic loading, the response of a Kelvin foam with open cells is governed by cell edge stretching and that of a random foam with open Voronoi cells by cell edge bending. The geometrical imperfections considered include variations in cell-wall lengths and random perturbations in the initial positions of the vertices of each hexagon. In similar spirit, Grenestedt and Bassinet (1998) have used the finite

element method to explore the effect of a dispersion of cell shape on the shear and bulk modulus of a closed cell foam. They perturbed the shape of a flat-faced Kelvin structure in a random manner and found that both the shear and bulk moduli are relatively insensitive to a dispersion in cell shape.

The current literature lacks studies on the multi-axial yield surface of foams as

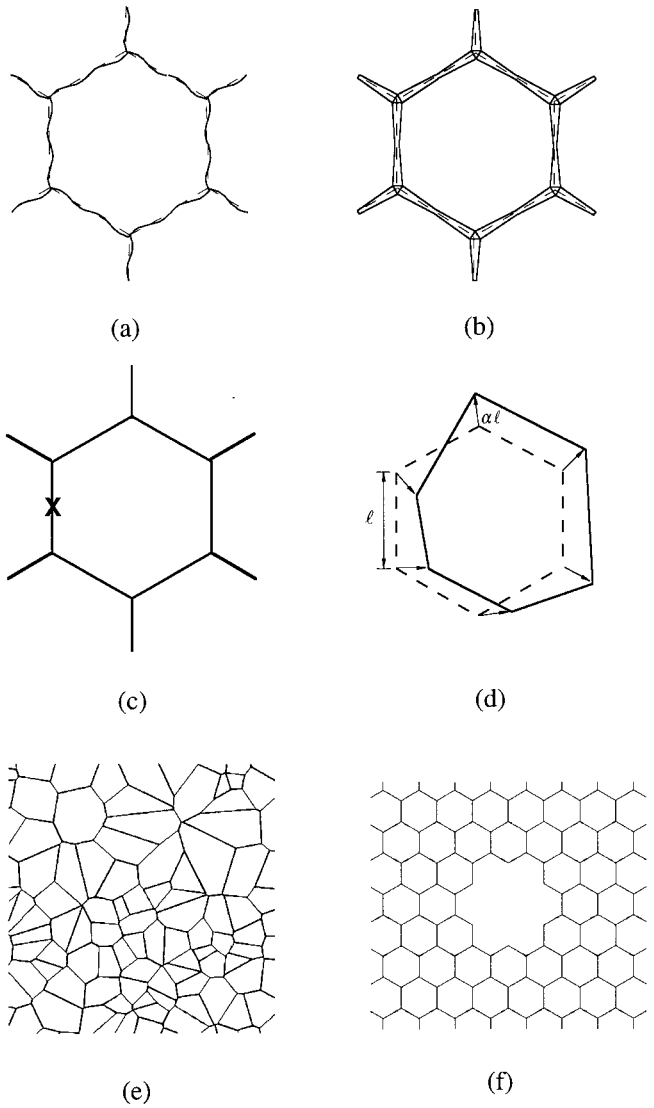

Fig. 1. Six different types of geometric imperfection considered in the present study: (a) waviness; (b) non-uniform wall thickness; (c) fractured cell walls; (d) cell-wall misalignment; (e) Voronoi structure; and (f) missing cells.

a function of random cellular structures, broken cell walls, cell wall misalignments and missing cells. It is also noted that in the studies of Silva et al. (1995) and Silva and Gibson (1997) for 2D Voronoi honeycombs and of Kraynik et al. (1997) for 3D Voronoi foams, the cell size distribution follows essentially the δ-distribution found in relatively uniform cellular microstructures. Recent image analysis on selected cross-sections of Alporas foams suggests that the cell size distribution is more closely described by the more random Γ-distribution (Klocker, 1998). The present paper is an attempt to study comprehensively the effects of various geometrical imperfections on the in-plane yielding behaviour of 2D cellular foams under biaxial loading by using a combination of analytical and finite element methods. Six different types of morphological defect are studied, as sketched in Fig. 1. First (in section 2), we address the reduction in strength of a regular honeycomb by the periodic imperfections of non-uniform wall thickness and cell wall waviness. Second (in section 3), the effects of random imperfections are determined: missing cell walls, a dispersion of cell size, cell wall misalignments and missing cells. In section 4, the numerically calculated yield surfaces are compared

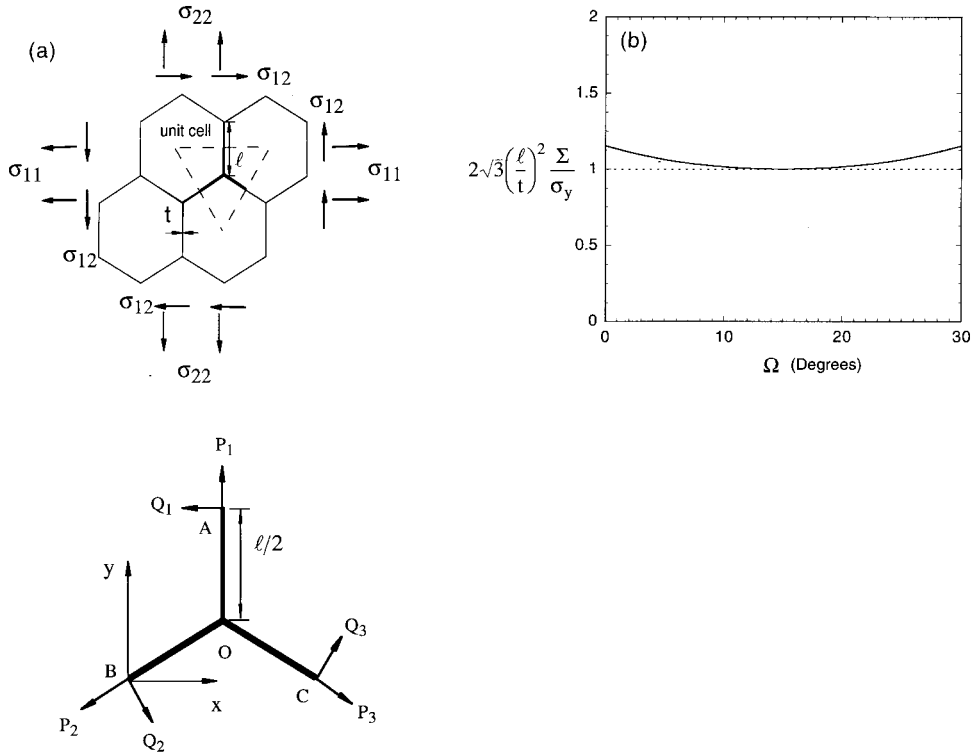

Fig. 2. (a) Unit cell model for ideal hexagonal honeycomb, and (b) dependence of the deviatoric yield strength Σ upon the inclination Ω of principal stresses relative to the microstrucure.

with a simple elliptical yield surface in order to provide support for the simple phenomenological model of yield as given by Deshpande and Fleck (1998).

2. Periodic imperfections

We adopt in this paper the same approach as that used by Silva et al. (1995), Silva and Gibson (1997), Kraynik et al. (1997), and Triantafyllidis and Schraad (1998) whereby each type of defect is studied separately for idealised cellular microstructures. Thus, our results should be considered at most as qualitative accounts of real metallic foams—these are nevertheless important for guiding the improvement of manufacturing processes and for future studies on the effects of defects on the yielding of real metallic foams. Periodic defects (wavy imperfections and non-uniform wall thickness) are studied in this section for regular honeycombs, whilst random defects (missing cell walls, cell-wall misalignments and random cell size distributions) are addressed in section 3.

2.1. Unit cell model

A unit cell approach is used, similar to that described by Warren and Kraynik (1987), to study the in-plane yielding response of an infinitely large regular honeycomb subjected to uniform stressing (Fig. 2). The reference honeycomb is a perfect, hexagonal structure with a cell wall length of l and a uniform cell wall thickness of t; cell wall waviness and non-uniform wall thickness are then introduced, as discussed below. The relative density $\bar{\rho}$ is given by $\bar{\rho} = 2t/\sqrt{3}l$. Results are presented below for regular honeycombs of sufficiently low relative density ($\bar{\rho} < 0.2$) that simple beam theory is adequate ($t/l < 0.2$). Symmetry indicates that the bending moment vanishes at the mid-point of each cell edge. The cell edges—OA, OB and OC in Fig. 2—are taken to be rigidly connected at joint O and are modelled by simple beam theory. It is further assumed that the cell wall material is rigid perfectly plastic with a yield strength denoted by σ_y. The axial and shear forces sustained by each beam are defined in Fig. 2 and satisfy the following equilibrium relations

$$P_1 - 1/2(P_2 + P_3) + \sqrt{3}/2(Q_3 - Q_2) = 0$$

$$-Q_1 - \sqrt{3}/2(P_3 - P_2) + 1/2(Q_3 + Q_2) = 0$$

$$Q_1 + Q_2 + Q_3 = 0. \tag{1}$$

These forces are related to the average macroscopic stresses (σ_{11}, σ_{22}, σ_{12}) by

$$P_i = \sqrt{3}lb(\sigma_{11} \cos^2 \theta_i + 2\sigma_{12} \cos \theta_i \sin \theta_i + \sigma_{22} \sin^2 \theta_i)$$

$$Q_i = \sqrt{3}lb[-\sigma_{11}\ \cos\ \theta_i\ \sin\ \theta_i + \sigma_{12}(\cos^2\theta_i - \sin^2\theta_i) + \sigma_{22}\ \cos\ \theta_i\ \sin\ \theta_i]$$

$$i = 1, 2, 3 \tag{2}$$

where b is the out-of plane thickness of the honeycomb. The angles θ_i denote the corresponding directions of the cell edges OA, OB and OC, and are given by

$$\theta_1 = \pi/2; \quad \theta_2 = 7\pi/6; \quad \theta_3 = 11\pi/6. \tag{3}$$

It is straightforward to check that the forces given by Eq. (2) satisfy the equilibrium Eq. (1).

The yield strength of a honeycomb is determined by studying the yield behaviour of the cell edges in the unit cell. Each cell edge is modelled as a cantilever beam clamped at one end and subjected to an axial force P and a transverse force Q at the free end. For a perfectly plastic solid, a plastic hinge appears at the clamped end when the forces satisfy the following yield condition (see, for example, Hodge, 1959)

$$|\ Ql\ |\ /2 - \sigma_y b[t^2/4 - P^2/(2\sigma_y b)^2] = 0. \tag{4}$$

Plastic collapse occurs when one or more plastic hinges appear in the unit cell, and this can be expressed by

$$|\ Q_i l\ |\ /2 - \sigma_y b[t^2/4 - P_i^2/(2\sigma_y b)^2] = 0 \quad \text{for } i = 1, 2 \text{ or } 3 \tag{5}$$

where P_i and Q_i (i = 1, 2, 3) are given by Eq. (2). It should be noted that the yield surface obtained from the unit cell model is the inner surface of the set of surfaces specified by Eq. (5). For the special case $\sigma_{12} = 0$, Eq. (5) reduces to

$$|\ \sigma_{11} - \sigma_{22}\ | = \frac{2\sigma_y t^2}{3l^2}\left[1 - 3/16(l/t)^2\frac{(3\sigma_{11} + \sigma_{22})^2}{\sigma_y^2}\right]. \tag{6}$$

If, on the other hand, the honeycomb is subjected to pure shear stressing, Eq. (5) becomes

$$|\ \sigma_{12}\ | = \frac{\sigma_y}{2\sqrt{3}}(t/l)^2. \tag{7}$$

Eqs. (6) and (7) are identical to those given by Gibson and Ashby (1997).

It should be noted that the *elastic* response of an ideal hexagonal honeycomb is isotropic. It is instructive to explore the degree of *plastic* anisotropy by subjecting the honeycomb to macroscopic deviatoric loading, comprising the principal stresses (Σ, $-\Sigma$) rotated by an angle Ω ($0 \le \Omega \le 90^\circ$) from the 1–2 axes of the honeycomb. The procedure is to resolve the principal stresses (Σ, $-\Sigma$) back into the stress components (σ_{11}, σ_{22}, σ_{12}) by Mohr's circle and then to evaluate the magnitude of Σ from Eqs. (2) and (5). Because an ideal hexagonal honeycomb has 6-fold symmetry, the calculated dependence of Σ upon Ω is plotted in Fig. 2(b) for

Ω in the range 0° to 30°. The honeycomb has a maximum strength for the orientation $\Omega = 0^\circ$ and 30°,

$$\Sigma = -2\sigma_y + 2\sigma_y\sqrt{1 + \frac{1}{3}(t/l)^2} \tag{8}$$

which can be approximated as

$$\Sigma = \frac{\sigma_y}{3}(t/l)^2 \tag{9}$$

when $(t/l)^2$ is small. The minimum strength exists for $\Omega = 15^\circ$ and is given by

$$\Sigma = \frac{\sigma_y}{2\sqrt{3}}(t/l)^2. \tag{10}$$

Fig. 2(b) reveals that the degree of plastic anisotropy is small for the ideal

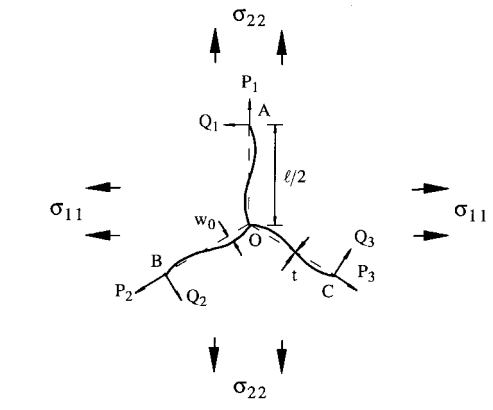

(a)

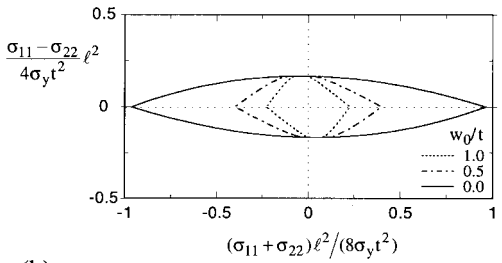

(b)

Fig. 3. (a) Unit cell of regular honeycomb with cell wall waviness, and (b) its yield surface for the case t/l and selected values of w_0/t.

hexagonal honeycomb. Thus, in the sequel, we will simplify the loading on perfect and imperfect honeycombs to principal stresses (σ_{11}, σ_{22}) aligned with the symmetry directions of the honeycomb.

The results presented above for a perfect honeycomb are taken as the reference in order to study the influence of two types of geometrical imperfection, wiggles and non-uniform wall thickness, on the yield surface. The analysis assumes that each cell wall contains identical imperfections which can be either wiggles or non-uniform wall thickness but not both.

2.2. Wavy cell edges

For simplicity, a wavy imperfection along each cell is described by the initial transverse deflection $w(x)$:

$$w = w_0 \sin(2n\pi x/l) \tag{11}$$

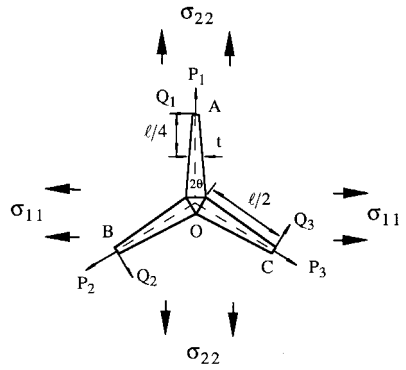

(a)

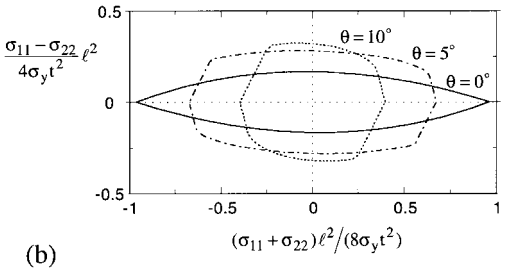

(b)

Fig. 4. (a) Unit cell of a perfect honeycomb with non-uniform wall thickness, and (b) its yield surface for the case $t/l = 0.15$ and selected values of w_0/t.

where w_0 is the amplitude of the waviness, n is the number of ripples in a length $l/2$, and x is the distance from the mid-joint O along the cell edge (Fig. 3(a)). Consider a wavy beam of length $l/2$ and thickness t which is clamped at one end, and is subjected to a transverse force Q and an axial force P at the other end; then, the yield locus in (P, Q) space is given by

$$| Q(l/2 - x_c) + Pw_c | - \sigma_y b \left[t^2/4 - \frac{(P \cos \varphi_c + Q \sin \varphi_c)^2}{(2\sigma_y b)^2} \right] = 0. \tag{12}$$

In the above equation, it is assumed that plastic collapse is by the formation of a plastic hinge at a distance x_c from the fixed end O; the initial transverse deflection and the associated slope at x_c are designated w_c and φ_c, respectively. The derivation of the yield condition and the method for determining (x_c, φ_c, w_c) are detailed in Appendix A. The effect of wavy imperfections on the yield surface, as predicted by Eqs. (2) and (12), is plotted in Fig. 3(b) for biaxial loading $(\sigma_{11}, \sigma_{22})$, with $t/l = 0.15$ and $n = 2$. It is seen that wavy imperfections reduce significantly the hydrostatic yield strength of a regular honeycomb but have only a minimal influence on its deviatoric yield strength—the resulting yield surface is much less elongated in biaxial macroscopic stress space when compared to that of a perfect honeycomb. For a fixed t/l ratio, an increase in the wave number n leads to a slight increase in the relative density and to no change in the macroscopic yield surface.

2.3. Non-uniform wall thickness

The effect of non-uniform wall thickness on the size and shape of the yield surface is now examined, using the simplified geometrical model shown in Fig. 4(a). It is assumed that the cell wall thickness decreases linearly from the joint O to the mid-point of the cell edge. The average cell edge thickness is denoted by t. Simple beam theory is employed, and so the predictions are limited to small variations in cell wall thickness. The yield surface for such an 'imperfect' honeycomb is obtained by analysing the plastic collapse of a clamped beam whose thickness varies linearly with length, as detailed in Appendix B. The critical load for collapse of such a beam is given by

$$| (l/2 - x_c)Q | - \sigma_y b \left[t_c^2/4 - \frac{P^2}{(2\sigma_y b)^2} \right] = 0 \tag{13}$$

where x_c is the distance of the plastic hinge from the built-in end. The thickness t_c at x_c is given by

$$t_c = t_1 - 2x_c(t_1 - t_2)/l \tag{14}$$

where

$$t_1 = t + \frac{l \tan \theta}{4}; \quad t_2 = t - \frac{l \tan \theta}{4}. \tag{15}$$

The predicted yield surface of a honeycomb with selected Plateau border imperfections is shown in Fig. 4(b) for the case $t/l = 0.15$. Again, no remote shear stress σ_{12} is applied. The presence of non-uniform wall thickness in a periodic honeycomb decreases its hydrostatic yield strength but enhances its deviatoric yield strength—the resulting yield surface is again less elongated when compared to that of a perfectly periodic honeycomb.

We note from Figs. 3(b) and 4(b) that the yield surface of a perfectly periodic honeycomb bounds the yield surface of an imperfect periodic honeycomb with wavy cell edges but not the yield surface of an imperfect periodic honeycomb with non-uniform wall thickness. Thus, the conclusion reached by Triantafyllidis and Schraad (1998) that the yield surface of a perfectly periodic honeycomb provides an upper bound for the yield surfaces of honeycombs with microstructural

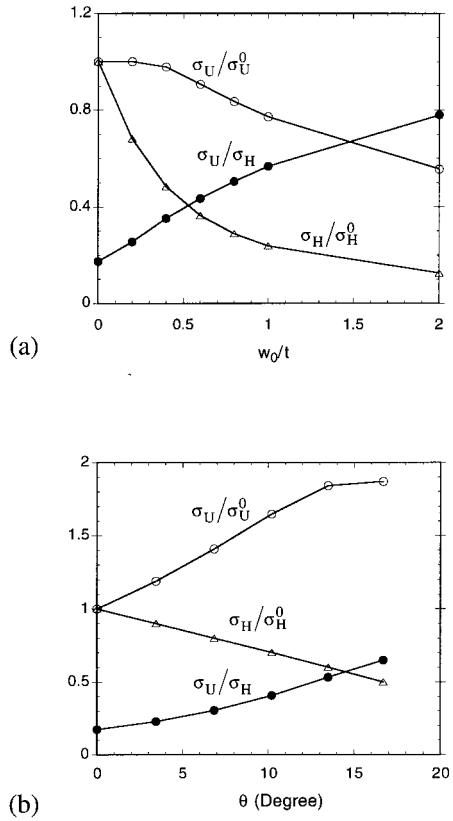

Fig. 5. Effects of (a) waviness and (b) non-uniform wall thickness on the yield strengths of perfect honeycombs.

imperfections is not universally applicable, at least, in the case where the imperfections are of the Plateau border (non-uniform cell wall thickness) type.

2.4. Reduction of yield strength due to periodic imperfections

It is well established that the deformation of an ideal honeycomb is governed by cell-edge bending under uniaxial stressing, and by cell-edge stretching under hydrostatic stressing. We shall now show that the presence of a small amount of cell wall waviness gives rise to a bending dominated deformation state under both uniaxial and hydrostatic loading. The uniaxial yield strength σ_U and the hydrostatic yield strength σ_H of a wavy honeycomb, normalised by the corresponding yield strengths σ_U^0 and σ_H^0 of a perfect honeycomb, are plotted as functions of cell-wall waviness amplitude w_0/t in Fig. 5(a), for a cell-wall thickness to length ratio $t/l = 0.15$. For completeness, the ratio of uniaxial to hydrostatic yield strength σ_U/σ_H of the imperfect honeycomb is included in the figure.

The presence of wavy imperfections changes the deformation mechanism under hydrostatic stressing from cell-edge stretching to cell-edge bending when the amplitude of waviness is only about the thickness of the cell wall; the corresponding drop in hydrostatic yield strength is significant—$\sigma_H/\sigma_H^0 \approx 0.2$ for $w_0/t \geq 1$. Wavy imperfections, on the other hand, lead to only a relatively small drop in uniaxial yield strength—$\sigma_U/\sigma_U^0 \approx 0.8$ when $w_0/t \approx 1$—which is expected as the deformation state of both ideal and wavy honeycombs are dominated by cell-edge bending under uniaxial stressing. Consequently, at $w_0/t \approx 1$, the uniaxial yield strength of the imperfect honeycomb is about 60% of its hydrostatic yield strength ($\sigma_U/\sigma_H \approx 0.6$), as opposed to $\sigma_U/\sigma_H \approx 0.18$ in the absence of imperfections.

In similar manner, the effects of the Plateau border parameter θ upon σ_U/σ_U^0, σ_H/σ_H^0 and upon σ_U/σ_H are shown in Fig. 5(b), for the case $t/l = 0.15$. The corresponding relative density of the honeycomb is 17.3%. The presence of non-uniform wall thickness decreases the hydrostatic yield strength σ_H slightly and increases the uniaxial yield strength σ_U slightly. This can be explained as follows. Under hydrostatic stressing, the deformation is governed by cell-wall stretching, but its yield strength is reduced due to thinning of the cell edges near their midpoints. Thus, the hydrostatic yield strength σ_H^0 of an ideal honeycomb provides an upper bound to the hydrostatic yield strengths of the honeycomb with non-uniform wall thickness, given that the relative density of the honeycombs remains unchanged. For the case of uniaxial stressing, yield is by the formation of a plastic hinge at the triangular joint; upon redistributing cell wall material in the vicinity of the joint, the plastic collapse moment increases and the macroscopic uniaxial strength increases. Hence, at fixed relative density, the uniaxial yield strength of a honeycomb with non-uniform wall thickness exceeds σ_U^0, as shown in Fig. 5(b). We conclude that σ_U^0 is *not* an upper bound for the uniaxial yield strengths of honeycombs with microstructural imperfections in the form of non-uniform wall thickness.

3. Random imperfections

In this section, a finite element method is used to study the effects on the yield behaviour of 2D foams for four types of random imperfection—fractured cell walls, cell-wall misalignments, missing cells, and a Voronoi distribution in cell size. Combined with the study presented in section 2, the overall aim is to identify those morphological imperfections which have a pernicious effect upon yield, and thereby to provide guidelines for the manufacture of metallic foams.

First, we consider the multi-axial yield response of foams with Voronoi distributions of cell size. The effects of cell wall misalignments, fractured cell walls and missing cells are then explored in turn. To create cell-wall misalignments, the joints of an ideal hexagonal honeycomb are displaced by a fixed amount in random directions. Fractured cell edges are introduced randomly for both regular

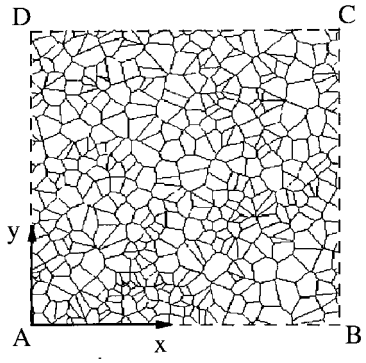

(a)

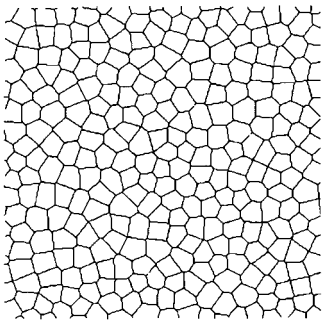

(b)

Fig. 6. Typical finite element mesh for the unit cell of a periodic Voronoi structure with (a) Γ-distributed cells and (b) δ-distributed cells.

honeycombs and for Voronoi structures. Missing cells are obtained by deleting one or more triangular joints in an ideal honeycomb and in a honeycomb already weakened by randomly distributed broken cell walls.

3.1. Voronoi cell models

If all pores nucleate simultaneously but randomly in space and grow at the same linear rate, the resulting structure is a Γ-Voronoi foam with a random morphological structure (Gibson and Ashby, 1997). Voronoi diagrams have been employed to study the elastic and uniaxial yield behaviours of 2D random honeycombs (Silva et al., 1995; Silva and Gibson, 1997) and the finite elastic deformation of 3D random foams (Kraynik et al., 1997). To create a 2D Voronoi diagram, randomly generated nucleation points are placed in a 2-dimensional domain according to an assumed distribution function. The domain is then divided into Voronoi polygons by drawing lines from each point to the nearest-neighbouring points, with normals drawn to bisect these lines. The area surrounding each generation point enclosed by the normals constitutes the Voronoi cell. It is assumed that the Voronoi diagram used in the present finite element model is the 'unit' cell of an infinite periodic cellular material with random microstructures, see Fig. 6(a). Thus, for any nucleation point K lying outside the unit cell ABCDA of size $L \times L$, its position is determined by a corresponding random point k in ABCDA through

$$x_K = x_k \pm mL$$

$$y_K = y_k \pm nL \tag{16}$$

where m and n are integers. In the current study these random nucleation points are generated using the commercial software Mathematica™. The resulting Voronoi diagram is then a globally periodical structure having a unit cell of size $L \times L$. With the assumption that all cell walls have the same thickness, t, the relative density $\bar{\rho}$ of the structure is given by

$$\bar{\rho} = \frac{t\Sigma l_k}{L^2} \tag{17}$$

where l_k are the cell-wall lengths and the summation is carried over the total number of cell walls within the unit cell.

The relative density of the model foam is changed by altering the cell wall thickness. In the finite element analysis, each cell wall is modelled by 1–13 Timoshenko beam elements (B22 element of ABAQUS), depending on the thickness to length ratio. It is found that the thickness to length ratio of a very few cell walls of the random microstructures (Γ-Voronoi, δ-Voronoi, and honeycombs with misalignments) exceeds 0.5. Generally speaking, continuum elements instead of beam elements should be used for these stocky cell walls. However, when the number fraction of short cell walls with respect to the total

number of cell walls is less than 5% (which is satisfied in all the cases studied here), the error incurred by modelling all cell walls in a random microstructure with beam elements is expected to be small.

The total degrees of freedom in a typical finite element model is in the range 35,000–70,000, depending on the total number of random Voronoi cells used in the representative cell—a mesh sensitivity study has been carried out and will be discussed further below. Unless otherwise stated, J_2-flow theory is employed and the cell wall material is assumed to be elastic-perfectly plastic with a Young's modulus of $E = 68$ GPa, a Poisson's ratio of $\nu = 0.3$, and a yield stress of $\sigma_y = 130$ MPa, which are representative of aluminium alloys. Thus, the independent non-dimensional material parameters are the Poisson's ratio ν and the yield strain $\sigma_y/E = 0.00191$. Furthermore, to ensure that the random structure has approximately isotropic properties, the unit cell is accepted only if its Young's modulus calculated from the finite element model varies within 4% in two orthogonal directions (the x and y directions in Fig. 6(a)).

3.1.1. Cell size distributions

A typical periodic unit cell ABCDA of size $L \times L$ arbitrary units and consisting of about 400 Voronoi polygons is shown in Fig. 6(a). Since this Voronoi diagram is generated without placing any constraints on the minimum distance between neighbouring random points, the resulting cell size distribution follows the Γ-distribution for which the probability of finding a cell of size a is given by

$$p(a) = \frac{\tau^\tau}{\bar{a}\Gamma(\tau)}\left(\frac{a}{\bar{a}}\right)^{\tau-1} \exp\left(-\tau\frac{a}{\bar{a}}\right) \tag{18}$$

where $\bar{a} = \langle a \rangle$ is the average cell size, Γ is the Gamma function and $\tau = 3.61$, as obtained by Weaire et al. (1986). If, however, the constraint is imposed that the separation between all nucleation points must exceed a minimum distance, the resulting Voronoi diagram has a nearly uniform cell size distribution given by the δ-distribution, as shown in Fig. 6(b). In their studies on Voronoi foams, Silva et al. (1995), Silva and Gibson (1997) and Kraynik et al. (1997) all make use of such a constraint to generate Voronoi diagrams. In this paper, both types of cell size distribution are considered and their effects on biaxial yielding of cellular foams are determined. The Voronoi cells are assumed to have uniform thickness and, in the case of the δ-distribution, it is further assumed that all cell walls must have a length at least three times the cell wall thickness. In addition, to provide baseline solutions, finite element calculations are performed on ideal hexagonal honeycombs of size $L \times L$ and the results are compared with those obtained from the unit cell analysis described in section 2.

3.1.2. Boundary conditions

Before performing any calculations, one must decide upon the most appropriate boundary conditions in the finite element model. The chosen boundary conditions should lead to the average global behaviour of the 2D foam, and not to localised

deformation near the boundaries of the mesh. We shall explore the effects of the boundary conditions upon the elastic-plastic response for both Voronoi foams and ideal honeycombs, and compare the predictions with the analytic results for an infinite ideal honeycomb.

Three types of boundary condition are considered in turn: (i) mixed boundary conditions, representative of frictionless grips (Fig. 7(a)); (ii) prescribed displacement boundary conditions, representative of sticking grips (Fig. 7(b)); and (iii) periodic boundary conditions (Fig. 7(c)). The mixed boundary conditions are enforced by prescribing the normal displacement along each edge of the mesh, with vanishing tangential force and bending moment at the edge nodes of the

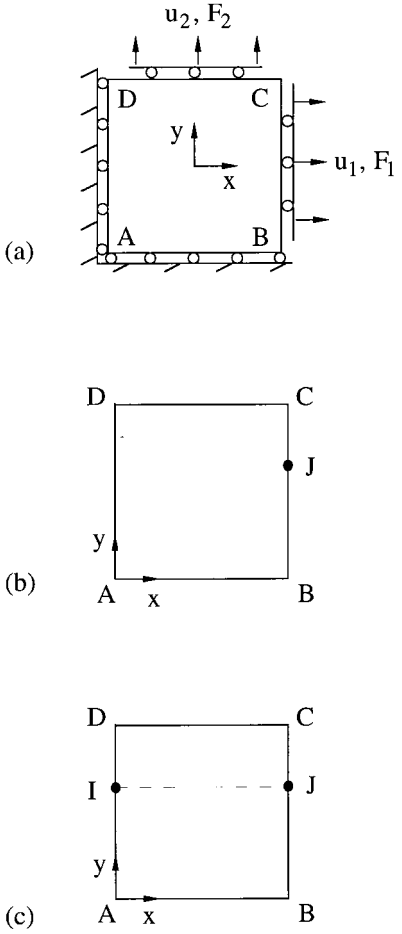

Fig. 7. Three different types of boundary condition: (a) mixed boundary conditions, (b) prescribed displacement boundary conditions, and (c) periodic boundary conditions.

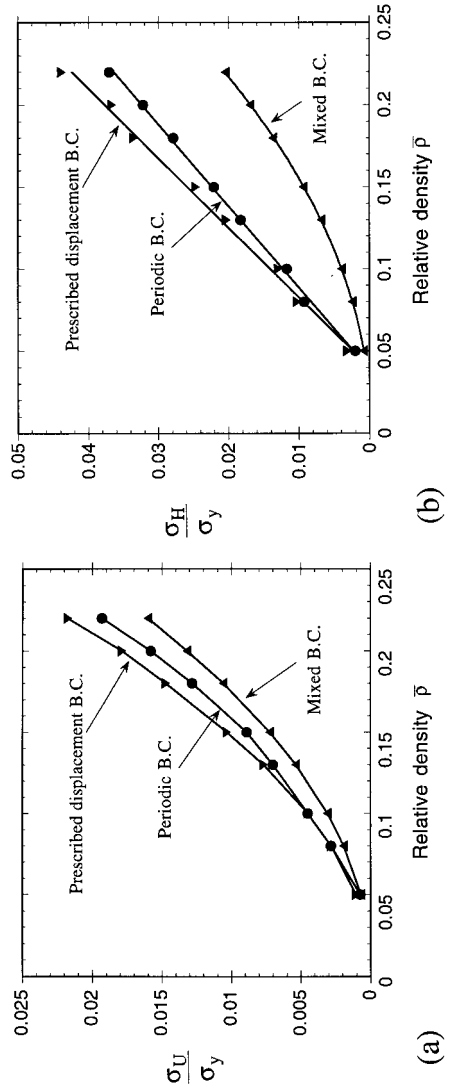

Fig. 8. Effect of choice of boundary conditions on (a) uniaxial and (b) hydrostatic yield strength of a Γ-distributed Voronoi structure.

finite element mesh. Boundary conditions of mixed type have been used previously by Silva et al. (1995), Silva and Gibson (1997), and Triantafyllidis and Schraad (1998).

Prescribed displacement boundary condition (sticking grips) requires that the translation displacements u_α^{J} and rotation θ^{J} of every node on the boundary ABCDA of Fig. 7(b) satisfy

$$u_\alpha^{\mathrm{J}} = \varepsilon_{\alpha\beta} x_\beta^{\mathrm{J}}, \quad \theta^{\mathrm{J}} = 0, \quad \alpha, \beta = 1, 2 \tag{19}$$

where $\varepsilon_{\alpha\beta}$ is the average macroscopic strain, x_β^{J} are the co-ordinates of a

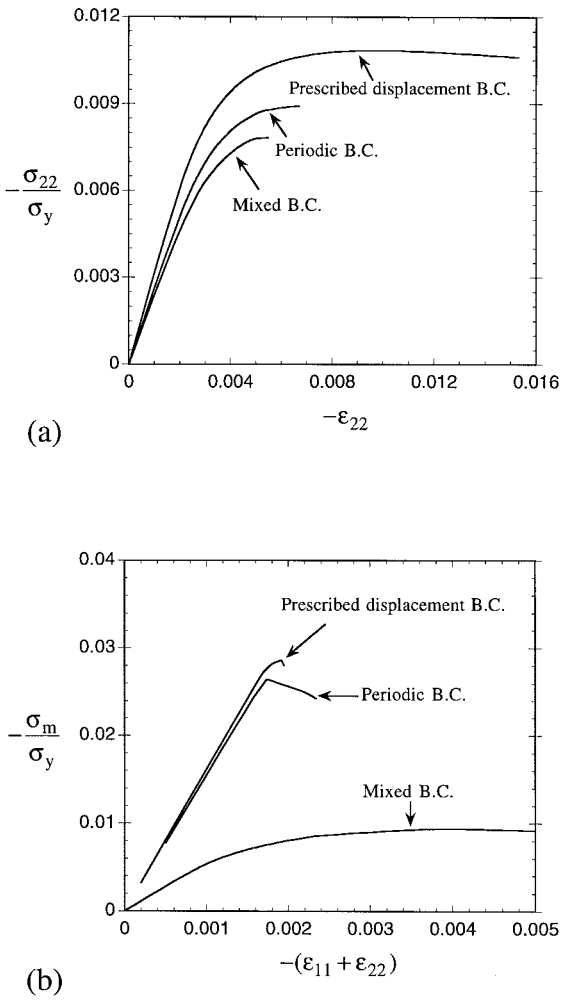

Fig. 9. Effect of choice of boundary conditions on (a) uniaxial, (b) hydrostatic stress vs strain behaviour of a Γ-distributed Voronoi structure with $\bar{\rho} = 0.15$.

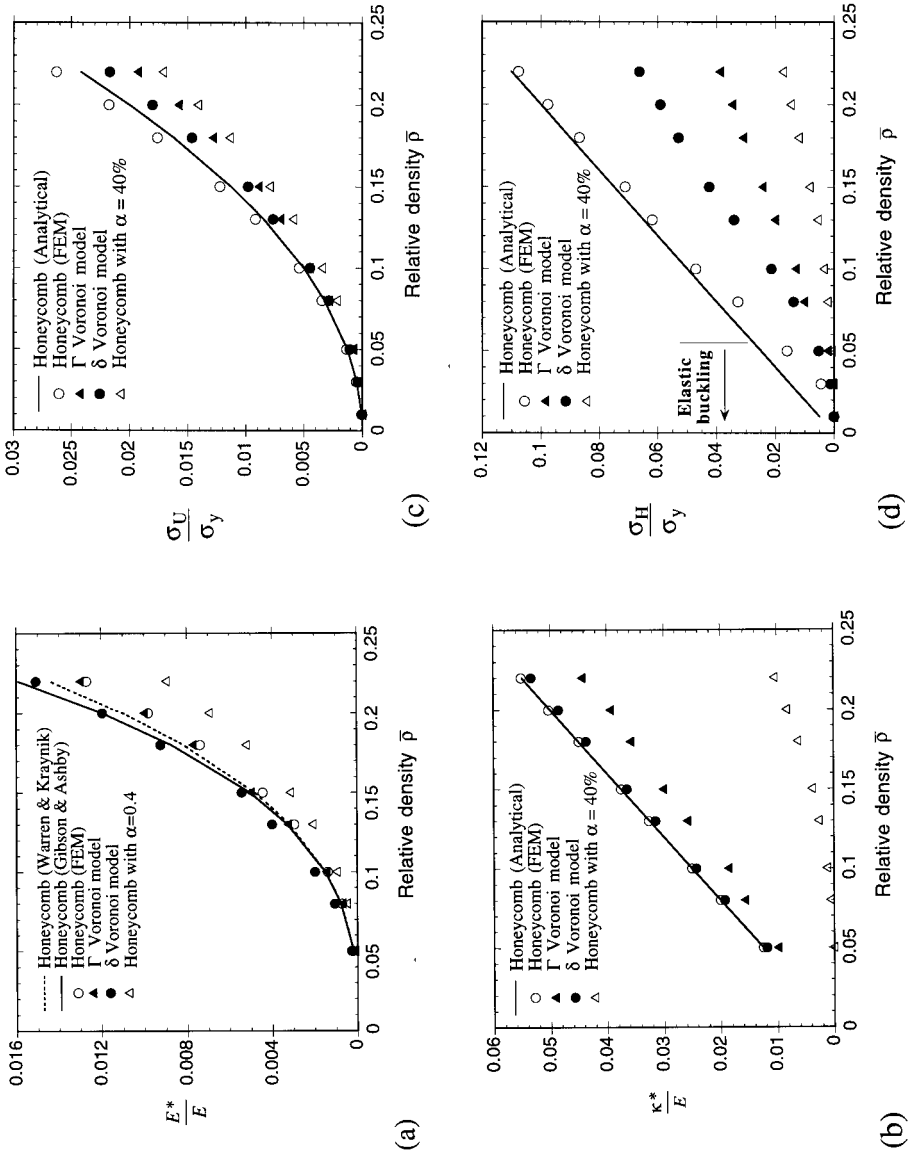

Fig. 10. Effect of all size variations and cell-wall misalignments on: (a) Young's modulus; (b) bulk modulus; (c) uniaxial yield strength; and (d) hydrostatic yield strength of 2D cellular foams.

representative node J on ABCDA, and the summation convention applies over repeated suffices. The corresponding macroscopic stresses are derived by

$$\sigma_{\alpha\beta} = \frac{1}{2L^2}\Sigma(x_\alpha^{\mathrm{J}} F_\beta^{\mathrm{J}} + x_\beta^{\mathrm{J}} F_\alpha^{\mathrm{J}}) \tag{20}$$

where F_α^{J} are the reaction forces on node J and the summation is carried over all nodes along ABCDA. Similarly, periodic boundary conditions on ABCDA imply

$$u_\alpha^{\mathrm{J}} - u_\alpha^{\mathrm{I}} = \varepsilon_{\alpha\beta}(x_\beta^{\mathrm{J}} - x_\beta^{\mathrm{I}}), \quad \theta^{\mathrm{J}} - \theta^{\mathrm{I}} = 0, \quad \alpha, \beta = 1, 2 \tag{21}$$

for pairs of nodes I and J on opposite edges of the mesh, as shown in Fig. 7(c). Without loss of generality, the shear strain ε_{12} is taken to be zero in the finite element calculation for the isotropic random structure. Moreover, proportional loading is applied by fixing the ratio $\varepsilon_{11}/\varepsilon_{22}$ except for the case of uniaxial loading cases for which ε_{11} is incremented with $\sigma_{22} = 0$.

The effects of the boundary conditions on the yield strength of a Γ-Voronoi foam are demonstrated in Fig. 8; here, the normalised uniaxial and hydrostatic compressive yield strengths ($\sigma_{\mathrm{U}}/\sigma_y$ and $\sigma_{\mathrm{H}}/\sigma_y$) are plotted as functions of relative density $\bar{\rho}$. The yield strength of the foam is defined by the peak on the stress versus strain curves, as shown in Fig. 9 for the case $\bar{\rho} = 0.15$. From Figs. 8 and 9 it is clear that the calculated yield strength of the Γ-Voronoi model is sensitive to the type of boundary condition imposed. On taking the periodic boundary condition as the most appropriate for the averaged response, the prescribed displacement boundary condition tends to overestimate the yield strength whilst the mixed boundary condition underestimates it. These results have practical significance. In the mechanical testing of honeycombs and foams, the imposed boundary conditions on a specimen approximate mixed boundary conditions for the case of frictionless grips, and displacement boundary conditions for the case of sticking grips. Such tests attempt to measure the bulk response of the foam, as given by periodic boundary conditions. Thus, a surface effect on the measured strength of the foams can be present in measurements. It is suggested that experiments be performed with frictionless grips and sticking grips in order to determine experimentally the influence of the boundary conditions on the strength.

For a perfect honeycomb, the normalised Young's modulus (E^*/E), bulk modulus (κ^*/E), uniaxial and hydrostatic compression yield strengths ($\sigma_{\mathrm{U}}/\sigma_{\mathrm{y}}$ and $\sigma_{\mathrm{H}}/\sigma_y$) obtained by the finite element method are plotted as functions of $\bar{\rho}$ in Fig. 10. Here, the Young's modulus E^* and bulk modulus κ^* are evaluated at the first increment of loading and the periodic boundary conditions (21) are applied; identical results are obtained if the prescribed displacement boundary conditions (19) are used. For comparison, Fig. 10 includes the known analytical solutions for an ideal honeycomb (Gibson and Ashby, 1997), given by

$$E^*/E = 1.49\bar{\rho}^3; \quad \kappa^*/E = 0.25\bar{\rho}$$

$$\sigma_U/\sigma_y = 0.5\bar{\rho}^2; \quad \sigma_H/\sigma_y = 0.5\bar{\rho} \tag{22}$$

It is seen that the finite element results agree closely with the analytical solutions (22) except for the hydrostatic compression yield strength at low relative densities ($\bar{\rho} < 0.1$). This deviation can be explained by the fact that the elastic buckling strength of a perfect honeycomb subjected to hydrostatic loading is comparable to its hydrostatic yield strength for $\bar{\rho} < 0.1$ at the chosen value $\sigma_y/E = 0.00191$. The coupling between elastic buckling and plastic yielding leads to a lower hydrostatic strength than that given in (22) for plastic yielding alone. Although not shown here, the yield surface of a perfect honeycomb has also been calculated using the periodic boundary condition and again it is found that the finite element results agree closely with the analytical predictions presented in section 2.

When the mixed boundary condition instead of periodic boundary condition is used in the finite element model for a perfectly periodic honeycomb, nearly identical results are obtained to those shown in Fig. 10 for uniaxial elastic and plastic properties. Under hydrostatic loading, the results are sensitive to whether the boundary cells of the finite element mesh are open or closed. For a mesh with closed-cell boundaries, the finite element model reproduces the analytical solutions (22); with open-cell boundaries, the cell walls of the open cells bend and crush at premature load levels, leading to a much lower bulk stiffness and hydrostatic yield strength compared to the predictions of (22). The above results suggest that it is important to apply the periodic boundary condition (21) for a mesh containing open cells at the boundaries. Therefore, in the remainder of this paper, only results using periodic boundary conditions will be reported.

3.1.3. Mesh sensitivity

A mesh sensitivity study has been performed by changing the total number N of random Γ-Voronoi cells in the unit cell enclosed by ABCDA. For each value of N, finite element calculations were performed for Voronoi diagrams generated

Table 1
Effect of number of cells on the calculated stiffness and strength of a Γ-distributed Voronoi structure with $\bar{\rho} = 15\%$[a]

Number of cells	κ^*/E	σ_H/σ_y	E^*/E	σ_U/σ_y
400 (a)	0.0299	0.0268	0.00607	0.0106
400 (b)	0.0298	0.0239	0.00618	0.0103
400 (c)	0.0307	0.300	0.00587	0.0105
400 (d)	0.0304	0.0265	0.00640	0.0111
800 (a)	0.0295	0.0245	0.00619	0.0108
800 (b)	0.0287	0.0240	0.00616	0.0110
800 (c)	0.0297	0.0244	0.00573	0.0103
1200 (a)	0.0299	0.0236	0.00565	0.0105
1200 (b)	0.0301	0.0254	0.00548	0.0102

[a] (a), (b), (c) and (d) following the number of cells denote meshes generated with different random sets of nucleation points.

with different sets of random seeds. Table 1 compares the Young's modulus, bulk modulus, and uniaxial and hydrostatic compression yield strengths of Γ-Voronoi structures having an identical relative density, $\bar{\rho} = 0.15$, but a different total number of cells, $N = 400$, 800 and 1200. It is seen that fewer cells are needed to model the elastic behaviour than the plastic response. When at least 800 random cells are used, the variation of uniaxial and hydrostatic yield strengths is within 10% from one Voronoi realisation to the next. The finite element results given below have been averaged over four random realisations of Voronoi foam with the total number of cells fixed at $N = 800$ unless otherwise stated.

3.2. Effect of cell size distribution

As already discussed in section 3.1, the cell sizes of a random Voronoi honeycomb created without constraining the minimum distance separating two adjacent generation points follows the Γ-distribution law, consistent with the experimentally measured cell size distribution for Alporas foams (Klocker, 1998). If the constraint that the distance between any two random generation points is larger than a minimum prescribed value is enforced, the resulting Voronoi diagram has an almost uniform cell size following the δ-distribution law. The calculated Young's modulus, bulk modulus, uniaxial and hydrostatic compression yield strengths are plotted in Fig. 10 as functions of relative density, for random Voronoi honeycombs having either Γ- or δ-distributed cell sizes. Results for hexagonal honeycombs are included for comparison.

We note from Fig. 10 that the uniaxial elastic and plastic properties of random Voronoi models are well described by those of a perfect honeycomb, regardless of whether the cells are distributed according to the Γ- or δ-law. Similar results for the elastic properties of a Voronoi honeycomb having δ-distributed cell sizes are reported by Silva et al. (1995) for 2D foams and by Grenestedt and Tanaka (1998) for 3D foams. However, Silva et al. (1995) found a 30% reduction in the uniaxial compressive yield strength when compared to that of a perfect honeycomb. The difference between the present results and those of Silva et al. (1995) for δ-Voronoi models is believed to be attributable to the different boundary conditions used—periodic boundary conditions (21) are used in the present study whereas mixed boundary conditions are used by Silva et al. (1995). Numerical simulations were performed to check this: on employing the same boundary conditions as those of Silva et al. (1995) we find that the uniaxial compressive strength of the δ-Voronoi foam is about 30% weaker than that of the perfect honeycomb.

The analytical solution of Gibson and Ashby (1997) is shown in Fig. 10(a). It is obtained by assuming that the cell walls deform according to bending only—the effects of stretching and shear deformation are ignored (Gibson and Ashby, 1997). Warren and Kraynik (1987) obtained an alternative analytical solution by using Euler–Bernoulli beam theory which includes both bending and stretching effects but neglects shear deformation. As the stretching term introduces another deformation mechanism, the honeycomb becomes more compliant, with a reduced

Young's modulus E^* (shown in Fig. 10(a) as the dashed line) compared to the Gibson–Ashby result. The present finite element solutions for the regular honeycomb correctly include all three deformations modes—bending, stretching and shear—and predict the most complaint response. It is also observed from Fig. 10(a) that a δ-Voronoi structure is stiffer than a regular honeycomb, implying that randomising the microstructure does not necessarily make it more compliant.

The normalised bulk modulus κ^*/E and hydrostatic yield strength σ_H/σ_y are presented in Figs. 10(b) and (d) as functions of the relative density $\bar{\rho}$ obtained for both Γ- and δ-distributed Voronoi structures with periodic boundary conditions. In Fig. 11, the dependence of the yield strength ratio σ_U/σ_H upon $\bar{\rho}$ is compared for Voronoi models and for ideal honeycombs. For a Voronoi structure having δ-distributed cell sizes, its bulk modulus κ^* is only slightly lower than that of a perfect honeycomb, but its hydrostatic yield strength σ_H is reduced significantly. Changing the cell size distribution from a δ- to Γ-law increases the level of imperfection in the cellular morphology, and leads to a further reduction in κ^* and σ_H. Although the hydrostatic elastic and plastic properties of a perfect honeycomb are significantly reduced by the presence of random cellular structures, the linear dependence of κ^* and σ_H on the relative density $\bar{\rho}$ as seen from Figs. 10(b) and (d) suggests that these morphological imperfections do not change the deformation mechanism from cell wall stretching to cell wall bending. This has been verified by changing the bending to stretching stiffness ratio for the Timoshenko beam elements—the finite element results for the Voronoi cell models remain unchanged if this ratio is changed by fixing the beam stretching stiffness while varying its bending stiffness, but not vice versa. Similarly, a change in the bending strength of the cell walls gives only a negligible change in the hydrostatic

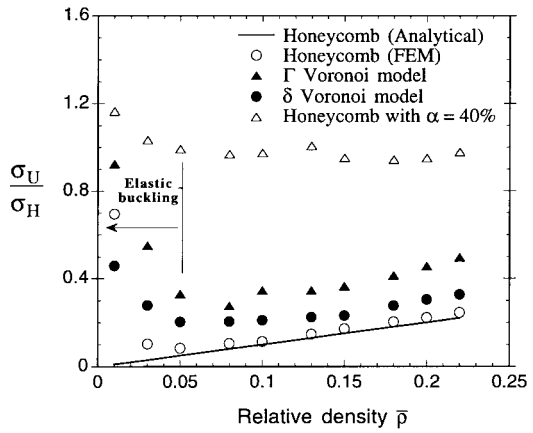

Fig. 11. Ratio of uniaxial to hydrostatic yield strength σ_U/σ_H vs relative density $\bar{\rho}$ for perfect honeycombs, Γ- and δ-distributed Voronoi structures, and honeycombs with cell-wall misalignments ($\alpha = 0.4$).

strength of the Voronoi structures, but a change in the stretching strength results in a proportional change in hydrostatic strength.

3.3. Effect of cell-wall misalignments

Cell-wall misalignments are believed to play an important rule in open-celled metallic foams having relatively regular morphological structure, e.g. Duocel foam, manufactured by ERG. Here, we limit our study to the effects of cell-wall

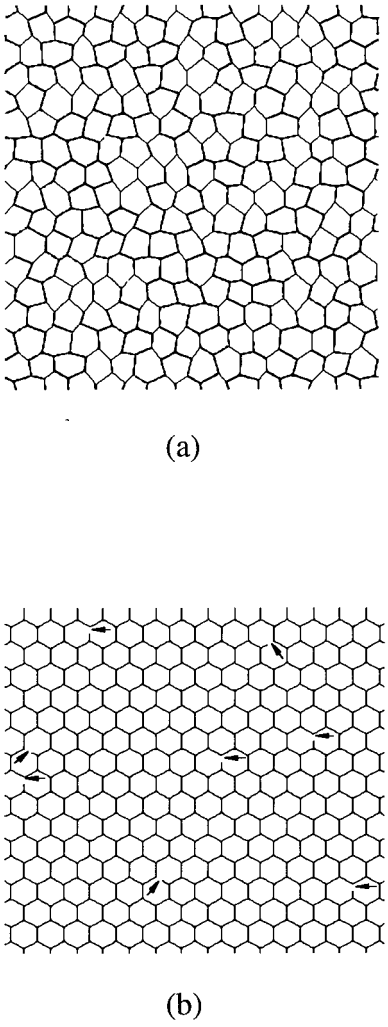

Fig. 12. Typical finite element mesh for honeycombs with (a) cell-wall misalignment ($\alpha = 0.2$), and (b) fractured cell walls (number fraction = 1%).

misalignments on the strength of hexagonal honeycombs using the finite element method.

The cell-wall misalignments are introduced by displacing in random directions the joints of a perfect hexagonal honeycomb by a constant distance αl, where l is the length of each side of the honeycomb, and the fraction α gives the magnitude of the imperfection. Thus, the co-ordinates (x_k, y_k) of a typical node are shifted to (x'_k, y'_k), as specified by

$$x'_k = x_k + \alpha l \cos\theta$$

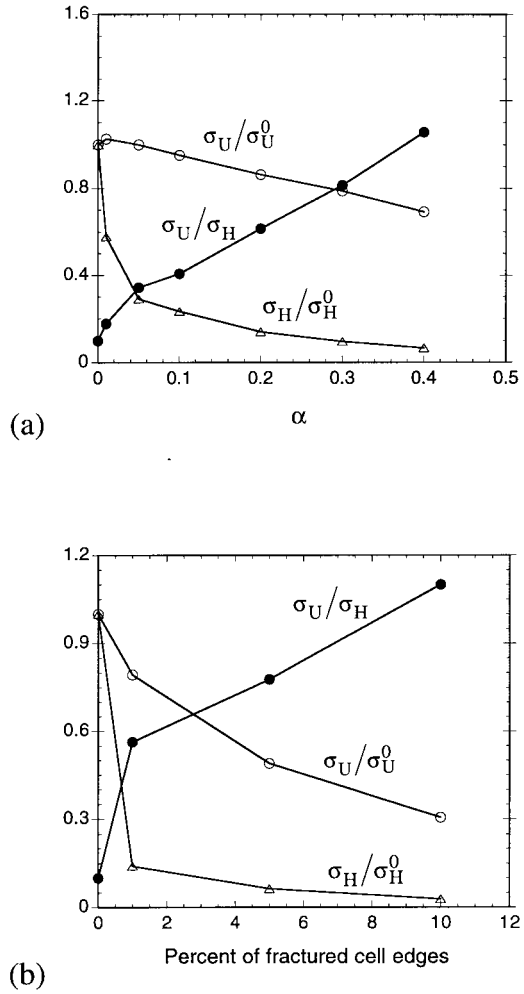

Fig. 13. Effect of (a) cell-wall misalignments, and (b) fractured cell walls on uniaxial and hydrostatic yield strengths of 2D foams with $\bar{\rho} = 0.1$.

$$y'_k = y_k + \alpha l \sin \theta \tag{23}$$

where θ is a random polar angle from the x-axis. The displaced cellular structure for the case $\alpha = 0.2$ is depicted in Fig. 12(a). Notice that, even at large misalignments ($\alpha = 0.2$), the cellular structure is still relatively uniform. The effects of the imperfection measure α upon the uniaxial and hydrostatic compression yield strengths are shown in Fig. 13(a) for a honeycomb of relative density $\bar{\rho} = 0.10$. The uniaxial yield strength is relatively insensitive to cell-wall misalignments, whereas the hydrostatic strength drops sharply with increasing α. By varying the bending to stretching strength ratio of a beam element, it is found that under hydrostatic stressing the deformation mechanism of cell-wall bending dominates over cell-wall stretching as the measure of misalignment α increases. Consequently, for $\alpha = 0.4$ the ratio σ_U/σ_H is nearly unity and is almost independent of $\bar{\rho}$, as shown in Fig. 11.

3.4. Effect of fractured cell walls

Fractured cell walls represent a common type of defects in commercial Al foams (Evans et al., 1998). Such a defect has been considered by Silva and Gibson (1997) who found that the random removal of some of the cell edges from a δ-distributed Voronoi honeycomb results in a sharp decrease of its uniaxial compression strength; a mixed boundary condition was used in their finite element model. Here, we explore both perfect honeycombs and Γ-Voronoi structures; periodic boundary conditions are employed throughout. Fig. 12(b) displays the finite element mesh of a perfect honeycomb with 1% of its cell edges removed randomly; the fractured cell edges are marked by small arrows on the mesh.

The uniaxial and hydrostatic yield strengths and their ratio are shown in Fig. 13(b) as functions of the percentage of fractured cell walls for an initially perfect honeycomb with $\bar{\rho} = 0.10$. The hydrostatic yield strength σ_H is much more sensitive to the presence of broken cell edges than the uniaxial yield strength σ_U; we note that a relatively small percentage (1%) of fractured cell walls reduces the value of σ_H sharply. Consequently, the uniaxial to hydrostatic yield strength ratio σ_U/σ_H approaches unity rapidly with increasing number of broken cell walls: the resulting yield surface is nearly a circle in biaxial macroscopic stress space. By varying the bending to stretching strength ratio of the beam elements, the bending of cell walls is found to be the dominant deformation mechanism under hydrostatic loading for perfect honeycombs with fractured cell walls. Recall that the hydrostatic compressive behaviours of Voronoi structures and perfect honeycombs without broken cell walls are dominated by cell-wall stretching.

The influence of broken cell edges on Γ-Voronoi models has also been studied, and it is found that the yield behaviour of a Γ-Voronoi structure with $\bar{\rho} = 0.10$ is essentially the same as that depicted in Fig. 13(b) for a perfect honeycomb. This is to be expected, as fractured cell walls have a much stronger knock-down effect than variations in cell size on the yield strength of 2D foams. Thus, when cell size variations co-exist with fractured cell walls in a 2D foam, the knock-down effect

on hydrostatic yield strength is overwhelmed by the presence of the fractured cell walls.

3.5. Effect of missing cells

The final type of imperfection considered is the missing cell. This is manifest in commercial metallic foams as large holes. The effect of missing cells on the Young's modulus, the elastic buckling strength and on the plastic yield strength of regular hexagonal honeycombs has been studied by Guo et al. (1999), using mixed boundary conditions. The buckling strength and yield strength are found to be more sensitive to the presence of holes than the elastic modulus. Here, we focus on the effects of large holes on the biaxial yield strength of perfectly periodic

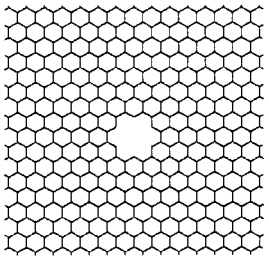

(a)

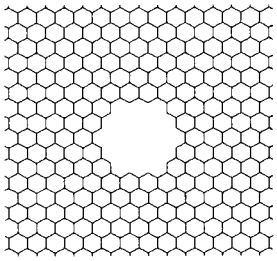

(b)

Fig. 14. Finite element mesh for a perfect honeycomb with (a) 1 cell missing, and (b) 7 cells missing.

honeycombs with or without other types of defect. Two hole sizes are considered, 1 missing cell (Fig. 14(a)) and 7 missing cells (Fig. 14(b)). The area fraction is $f = 3.1\%$ for 1 missing cell and $f = 8.5\%$ for 7 missing cells. The initial relative density of the honeycomb is fixed at $\bar{\rho} = 0.1$ and periodic boundary conditions are applied. As two or more different types of imperfections are likely to co-exist in a typical metallic foam, the combined effects of holes and fractured cell edges are also studied. The calculated uniaxial and hydrostatic yield strengths as functions

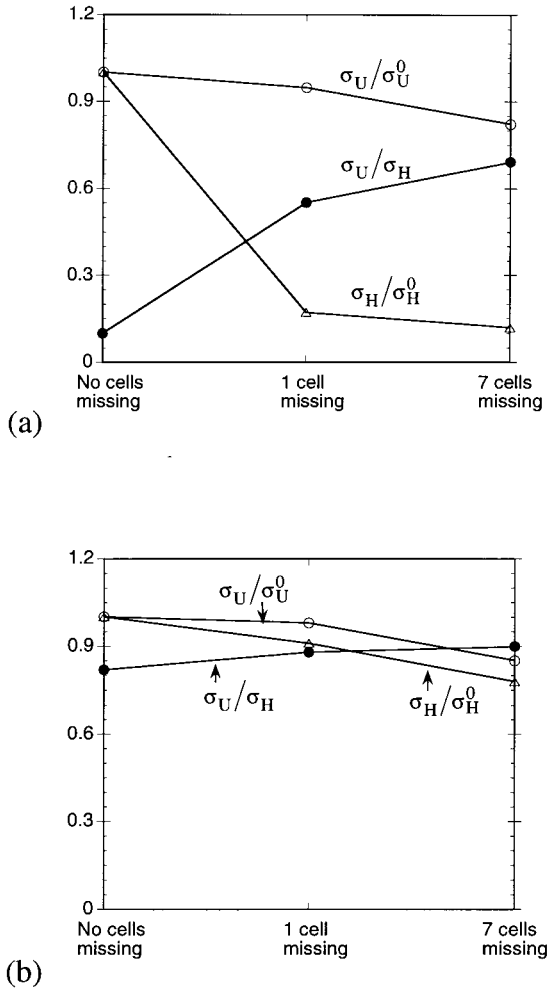

Fig. 15. Effect of the number of missing cells on uniaxial and hydrostatic yield strengths of (a) perfect honeycomb, and (b) perfect honeycomb with 5% fractured cell edges. The initial relative density of both honeycombs is $\bar{\rho} = 0.1$.

of hole size are shown in Fig. 15(a) for a honeycomb without fractured cell edges and in Fig. 15(b) for a honeycomb with 5% randomly distributed broken cell edges. In both figures the results for uniaxial and hydrostatic strengths are normalised by the values with no missing cells. Thus, in Fig. 15(b), the uniaxial strength σ_U^0 and the hydrostatic strength σ_H^0 refer to a honeycomb with 5% broken cell edges but no missing cells.

In the absence of other types of geometric imperfections such as broken cell edges, Fig. 15(a) reveals that the presence of a single hole has a strong knock-down effect on the hydrostatic strength of an initially perfect honeycomb and a smaller effect on its uniaxial yield strength. There is only a minor effect of hole size relative to the underlying hexagonal microstructure. A simple interpretation of these findings is that the presence of a hole induces bending of cell walls for hydrostatic loading, and thereby produces a large knock-down in strength. For the case of uniaxial compression, bending dominates the response with or without the presence of holes, and the presence of a hole has only a minor effect on the macroscopic strength.

The simultaneous effects of missing cells and random fractured cell edges are such that the foam is insensitive to the presence of isolated large holes when subjected to both uniaxial and hydrostatic loadings, see Fig. 15(b). This is in agreement with the experimental observation of Olurin et al. (1999) and Evans (1998) on aluminium metallic foams such as Alporas. Further studies are required in order to explore the precise dependence of macroscopic strength upon the volume fraction of holes and upon the size of holes relative to the underlying microstructure. The effects of rigid inclusions on multi-axial strength are also left to future study: redundancy defects in the form of solid inclusions are present in commercial metallic foams and contribute significantly to reduced strength to density ratios. The stress-concentrating effects of such defects may reduce strength in addition to increasing the mass of the foam.

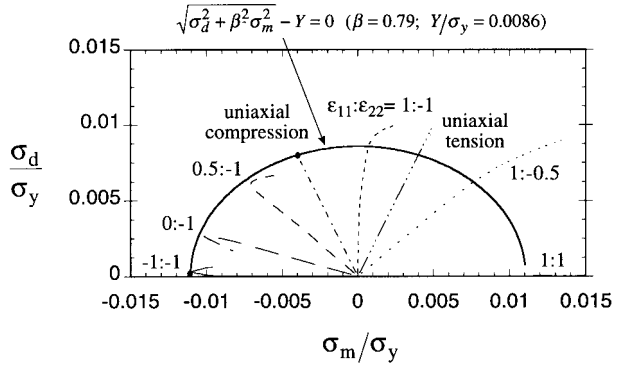

Fig. 16. Elliptical yield surface of a Γ-distributed Voronoi structure with 5% fractured cell edges fitted to the finite element calculated stress paths in the σ_d–σ_m space under proportional straining. The initial relative density of the foam is $\bar{\rho} = 0.15$.

4. Yield surface of 2D foams with imperfections

For 2D isotropic cellular solids with random microstructures, their yield behaviours are fully characterised by two stress invariants, the mean stress σ_m and the effective deviatoric stress σ_d, given by

$$\sigma_d = \sqrt{2 s_{\alpha\beta} s_{\alpha\beta}}; \quad \sigma_m = \frac{1}{2}\sigma_{\alpha\alpha}$$

$$s_{\alpha\beta} = \sigma_{\alpha\beta} - \delta_{\alpha\beta}\sigma_m; \quad \alpha, \beta = 1, 2 \tag{24}$$

The predicted loading paths in the σ_d–σ_m space under proportional straining is

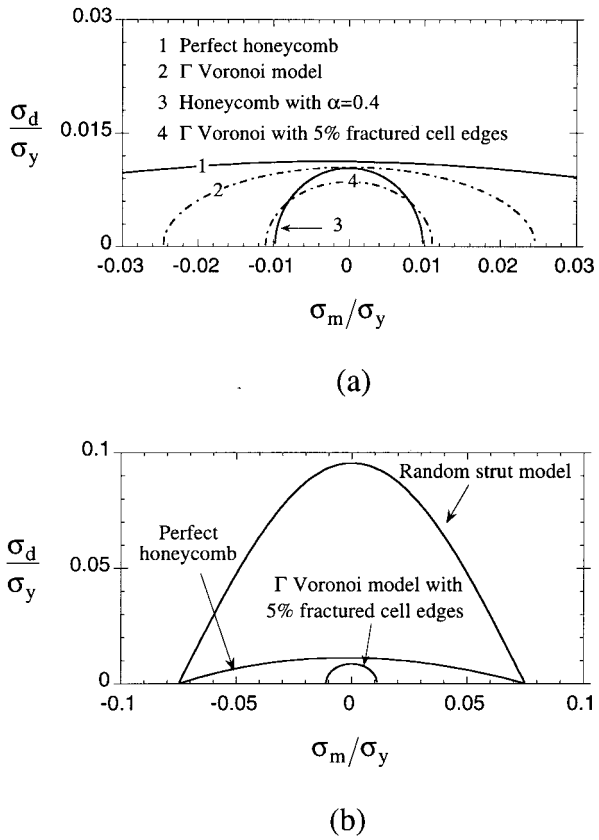

Fig. 17. (a) Typical elliptical yield surfaces of Γ-distributed Voronoi structures with and without fractured cell edges (5%) and perfect honeycombs with and without cell-edge misalignments ($\alpha = 0.4$); (b) Taylor yield surface of 2D random strut structures compared with the yield surfaces of perfect honeycombs and Γ-distributed Voronoi structures with 5% fractured cell edges. The relative density of the foams is fixed at $\bar{\rho} = 0.15$.

plotted in Fig. 16 for a Γ-distributed Voronoi structure with 5% fractured cell edges; a fixed relative density $\bar{\rho} = 0.15$ is assumed. We note that at least one component of the stress goes through a maximum when the mean stress is negative. An elliptical yield surface fits these limit points, as shown in Fig. 16. We can express this yield surface by

$$\bar{\sigma} - Y \leq 0 \tag{25}$$

where $\bar{\sigma}$ is an equivalent stress defined by

$$\bar{\sigma} = \sqrt{\sigma_{\mathrm{d}}^2 + \beta^2 \sigma_{\mathrm{m}}^2} \tag{26}$$

The material constants β and Y are related to the uniaxial and hydrostatic compressive yield strengths (σ_{U}, σ_{H}) by

$$\beta = \sqrt{\frac{4\sigma_{\mathrm{U}}^2}{4\sigma_{\mathrm{H}}^2 - \sigma_{\mathrm{U}}^2}}, \quad Y = \beta \sigma_{\mathrm{H}} \tag{27}$$

Note that the yield condition (25) reduces to the Mises yield criterion when $\beta = 0$.

Extensive finite element calculations have been carried out to establish the dependence of β and Y upon $\bar{\rho}$. The following relations are found to hold

$$\beta^2 = \xi \bar{\rho}, \quad Y/\sigma_y = \eta \bar{\rho}^2 \tag{28}$$

where ξ and η are constants depending on the type of morphological imperfection as well as the boundary conditions applied. (For practical applications, experimental measurements of ξ and η are recommended.) For example, for Γ-distributed Voronoi honeycombs with no fractured walls and loaded by periodic boundary conditions, we find that $\xi = 1.2$ and $\eta = 0.47$. Similar calculations have been performed for a Γ-distributed Voronoi structure with 5% fractured cell walls and a honeycomb with cell-wall misalignment ($\alpha = 0.4$), both at a fixed relative density of $\bar{\rho} = 0.15$. The predicted yield surfaces of these imperfect 2D foams using (26) are presented in Fig. 17(a) and are compared with that for a perfect honeycomb. The results shown in Fig. 17(a) reveal that the yield surfaces of 2D foams with random imperfections are bounded by the yield surface of a perfect honeycomb.

It is instructive to compare the yield surface given above with that predicted by a Taylor upper bound calculation. To construct such a bound, we assume that the 2D foam comprises straight struts in all directions, with the ends of the struts subjected to affine deformation. Grenestedt (1997) used such a random strut model to study the yield surfaces of 3D model foam structures. Here, we use the upper bound method to derive the Taylor yield surface for 2D model structures (Appendix C). For $\bar{\rho} = 0.15$, the predicted Taylor yield surface is plotted in Fig. 17(b) and is compared with the yield surfaces of a perfect honeycomb and of a Γ-distributed Voronoi structure containing 5% fractured cell edges. The nearly circular shape of the Taylor yield surface is consistent with experimental

measurements (Deshpande and Fleck, 1998; Gioux et al., 1998) but its size is about an order of magnitude too large. This is to be expected, as the Taylor surface is derived (Appendix C) with the assumption that stretching, not bending, dominates the deformation of individual struts for all macroscopic stress states. A perfect honeycomb yields by cell-wall stretching under hydrostatic stressing and by cell-wall bending when subjected to uniaxial stressing, hence its yield surface appears elongated in the $\sigma_d-\sigma_m$ space, with a size smaller than that of the Taylor yield surface and larger than that of a Γ-distributed Voronoi structure with 5% fractured cell edges. Under predominantly deviatoric stressing, the struts in a perfect honeycomb undergo bending whereas the upper bound calculation assumes stretching. The struts in an imperfect Voronoi model with 5% fractures edges undergo bending deformation under all macroscopic stress states.

5. Concluding remarks

The effects of *periodic imperfections* (cell wall waviness and non-uniform wall thickness) in altering the shape and size of the yield surface have been examined analytically, using a unit cell model for periodic hexagonal honeycombs. Wavy imperfections reduce significantly the hydrostatic yield strength but have only a minimal influence on the deviatoric strength; non-uniform wall thickness, on the other hand, reduce slightly the hydrostatic yield strength and increase slightly the deviatoric strength.

Random imperfections, in the form of cell-size variations, fractured cell walls, cell-wall misalignments, and missing cells, have been addressed using the finite element method. Cell wall misalignments induce cell wall bending under hydrostatic loading and lead to a large reduction of hydrostatic strength. Similarly, the removal of some of the cell walls leads to cell wall bending and to pronounced weakening. The effect of a random distribution of cell size on strength is addressed by considering the yield surface for δ- and Γ-Voronoi structures: although their hydrostatic strengths are less than that of a perfect honeycomb by a factor of 2 to 3, these microstructures are not sufficiently dispersed in cell size to switch the deformation response from cell wall stretching to cell wall bending under hydrostatic loading. Consequently, the hydrostatic strength of the Voronoi models scales linearly with relative density whereas their deviatoric strength scales quadratically with relative density. These collected finite element results suggest that the yield surface of random 2D foams, when projected onto a space of equivalent deviatoric stress and mean stress, is much less elongated than that of regular honeycombs. The finite element method is also used to study the sensitivity of the yield strength to the assumed boundary conditions. Periodic boundary conditions give a stronger response than displacement boundary conditions, particularly under hydrostatic loading. This suggests that experimental measurements of the yield response of a foam may be sensitive to edge effects and not give a representative measure of the bulk response.

Fractured cell edges produce the largest knock-down in yield strength of 2D

foams, followed in order by missing cells, wavy cell edges, cell edge misalignments, Γ Voronoi cells, δ Voronoi cells, and non-uniform wall thickness. The nearly circular yield surfaces predicted for honeycombs with either fractured cell edges or cell-edge misalignments when plotted in combined deviatoric and mean stress space are confirmed by recent experimental observations by Deshpande and Fleck (1998) and Gioux et al. (1998). The Taylor yield surface, although circular in shape, is an order of magnitude larger in size than the experimental measurements. A simple elliptical yield function with two adjustable material parameters successfully fits the numerically predicted yield surfaces for the imperfect 2D foams, and shows potential as a phenomenological constitutive law to guide the design of structural components made of metallic foams.

Additional studies are required to assess the knock-down in strength due to redundancy defects in the form of rigid inclusions within the foam. Such defects are detrimental as they may reduce the strength in addition to increasing the mass of the foam.

Acknowledgements

This work was partially supported by the EPSRC and by the ARPA/ONR MURI program on Ultralight Metal Structures (No. N00014-1-96-1028). The authors wish to thank Professor M. F. Ashby for helpful discussions.

Appendix A

Yielding of a wavy beam

The yield condition for a wavy beam of length $l/2$ and thickness t, clamped at one end and subjected to a transverse force Q and to an axial force P at the other end, is given below. The initial waviness is given by Eq. (11). With the assumption that the plastic hinge appears at x_c, a distance measured from the clamped end, the axial force N and moment M at the plastic hinge are obtained as

$$N = P\ \cos\ \varphi_c + Q\ \sin\ \varphi_c$$

$$M = Q(l/2 - x_c) + Pw_c \tag{A1}$$

where φ_c and w_c are related to the unknown position x_c by

$$\varphi_c = \tan^{-1}\left(\frac{2n\pi w_0}{l}\cos\frac{2n\pi x_c}{l}\right)$$

$$w_c = w_0\ \sin\left(\frac{2n\pi x_c}{l}\right) \tag{A2}$$

Substituting Eq. (A1) into the yielding condition (4) results in

$$| Q(l/2 - x_c) + Pw_c | - \sigma_y b \left[t^2/4 - \frac{(P \cos \varphi_c + Q \sin \varphi_c)^2}{(2\sigma_y b)^2} \right] = 0 \tag{A3}$$

When $Q \neq 0$, x_c is determined by minimising the absolute value of Q for any given ratio of P/Q. In the limit $Q \to 0$, the plastic hinge must appear at $x_c = l/(4n)$, hence

$$P = \pm 2\sigma_y b(-w_0 + \sqrt{w_0^2 + t^2/4}) \tag{A4}$$

In the other limit when $P \to 0$, the plastic hinge forms at the clamped end, giving

$$Q = \pm \frac{\sigma_y b(-2l + \sqrt{(2l)^2 + 4t^2 \sin^2 \varphi_c})}{2 \sin^2 \varphi_c} \tag{A5}$$

where $\varphi_c = \tan^{-1}(2n\pi w_0/l)$. We assume that the beams are slender ($t \ll l$) and so Eq. (A5) can be approximated as

$$Q = \pm \frac{\sigma_y b t^2}{4l^2} \tag{A6}$$

Eq. (A4) suggests that the stretching strength of the beam is strongly dependent upon the magnitude of the wavy imperfection w_0 and independent of the wave number n, while Eq. (A6) implies that the bending strength of the beam is hardly affected by the presence of wavy imperfections.

Appendix B

Yielding of a beam with non-uniform wall thickness

Consider a clamped beam of length $l/2$ whose thickness changes linearly from the fixed end to the free end. For a given set of forces P and Q, the condition governing the formation of a plastic hinge at location x_c measured from the fixed end, is

$$| Q(l/2 - x_c) | - \sigma_y b[t_c^2/4 - P^2/(2\sigma_y b)^2] = 0 \tag{B1}$$

where

$$t_c = t_1 - 2x_c(t_1 - t_2)/l \tag{B2}$$

is the beam thickness at x_c, and t_1 and t_2 are the thickness of the beam at the clamped end and the free end, respectively, as defined by Eq. (15). When only P or Q is imposed, x_c can be determined directly. For the case $Q = 0$, it is

straightforward to show from (B1) that the plastic hinge forms at the free end (i.e. $x_c = 0$), with

$$P = \sigma_y b t_2. \tag{B3}$$

When $P = 0$, the position of the plastic hinge depends on the ratio t_1/t_2 as

$$\frac{x_c}{l} = \begin{cases} 0, & 1 \le t_1/t_2 \le 2 \\ \dfrac{t_1/t_2 - 2}{t_1/t_2 - 1}, & 2 \le t_1/t_2 < \infty \end{cases} \tag{B4}$$

and the corresponding bending strength is given by

$$Q = \begin{cases} \dfrac{\sigma_y b t_1^2}{4l}, & 1 \le t_1/t_2 \le 2 \\ \dfrac{\sigma_y b t_2 (t_1 - t_2)}{2l}, & 2 \le t_1/t_2 < \infty \end{cases}. \tag{B5}$$

When both P and Q are imposed at the free end, the plastic hinge position x_c must be determined numerically from (B1). From (B3) and (B5) it is seen that, for small geometric defects ($1 \le t_1/t_2 \le 2$), the Plateau border imperfection increases the bending strength and reduces its stretching strength when compared with a clamped cantilever beam of length $l/2$ and uniform thickness $t = (t_1 + t_2)/2$.

Appendix C

Taylor yield surface of 2D foams

We contemplate a model foam of volume V made of random struts in 2D space. It is assumed that the material is rigid, ideally plastic and that the deformation of each strut is dominated by stretching with negligible bending effects. The model structure is subjected to a uniform macroscopic strain rate field $\dot{\varepsilon}_{ij}$ and, without loss of generality for the isotropic structure, the Cartesian coordinate axes (x, y) are aligned with the principal axes of strain rate. With these assumptions, the stretching rate of an arbitrary strut oriented at angle θ from the x-axis is given by

$$\dot{\varepsilon} = \dot{\varepsilon}_1 \cos^2\theta + \dot{\varepsilon}_2 \sin^2\theta \tag{C1}$$

where $\dot{\varepsilon}_1$ and $\dot{\varepsilon}_2$ are the principal macroscopic strain rates. The rate of plastic dissipation per unit volume of the foam is

$$\dot{w}_p = \frac{1}{V}\int_V \sigma_y \mid \dot{\varepsilon} \mid \mathrm{d}V \tag{C2}$$

where V is the volume of the foam.

The macroscopic stress σ_α is given by $\sigma_\alpha = \partial \dot{w}_p / \partial \dot{\varepsilon}_\alpha (\alpha = 1, 2)$ and integrating (C2) over all directions gives

$$\sigma_1 = \frac{\bar{\rho}}{2\pi} \int_0^{2\pi} \sigma_y \, \mathrm{sign}(\varepsilon) \cos^2 \theta \, \mathrm{d}\theta$$

$$\sigma_2 = \frac{\bar{\rho}}{2\pi} \int_0^{2\pi} \sigma_y \, \mathrm{sign}(\varepsilon) \cos^2 \theta \, \mathrm{d}\theta \tag{C3}$$

where $\bar{\rho}$ is the relative density.

Explicit formulae for σ_α follow directly as

$$\sigma_1 = \pm 0.5 \sigma_y \bar{\rho}$$

$$\sigma_2 = \pm 0.5 \sigma_y \bar{\rho} \tag{C4}$$

for $\dot{\varepsilon}_1 \dot{\varepsilon}_2 \geq 0$, and

$$\sigma_1 = \sigma_y \bar{\rho} \frac{2\theta_c + \sin 2\theta_c - \pi/2}{\pi}$$

$$\sigma_2 = \sigma_y \bar{\rho} \frac{2\theta_c - \sin 2\theta_c - \pi/2}{\pi} \tag{C5}$$

for $\dot{\varepsilon}_1 \dot{\varepsilon}_2 < 0$. The angle θ_c is defined by $\theta_c \equiv \tan^{-1}(\sqrt{-\dot{\varepsilon}_1 / \dot{\varepsilon}_2})$. The predicted Taylor yield surface from (C4) and (C5) is plotted in the $\sigma_d - \sigma_m$ space in Fig. 17(b) for the case $\bar{\rho} = 0.15$. The above analysis is similar to that given by Fleck et al. (1992) for the yield surface of 3D metallic powders under axisymmetric loading.

References

ABAQUS Standard User's Manual, Version 5.6, 1997. Hibbitt, Karlsson and Sorensen, Inc., Providence, Rhode Island.

Deshpande, V.S., Fleck, N.A., 1998. A phenomenological constitutive model for metallic foams. Submitted to J. Mech. Phys. Solids.

Evans, A.G. 1998 private communication.

Evans, A.G., Hutchinson, J.W., Ashby, M.F. 1998 The thermostructural performance of cellular metal systems and components, to appear in Progress in Materials Science.

Fleck, N.A., Kuhn, L.T., McMeeking, R.M., 1992. Yielding of metal powder bonded by isolated contacts. J. Mech. Phys. Solids 40, 1139–1162.

Gibson, L.J., Ashby, M.F., Zhang, J., Triantafiliou, T.C., 1989. Failure surfaces for cellular materials under multi-axial loads—(I) Modeling. Int. J. Mech. Sci. 31, 635–665.

Gibson, L.J., Ashby, M.F., 1997. Cellular Solids: Structure and Properties, 2nd ed. Cambridge University Press, Cambridge.

Gioux, G., McCormack, Gibson, L.J., 1998. Failure of aluminium foams under multiaxial loads, submitted to Int. J. Mech. Sci.

Grenestedt, J.L. 1997 Effective yield behaviour of some models for perfect cellular solids. CUED Report, Cambridge University, Cambridge.

Grenestedt, J.L., 1998. Influence of wavy imperfections in cell walls on elastic stiffness of cellular solids. J. Mech. Phys. Solids 46, 29–50.

Grenestedt, J.L., Bassinet, F., 1998. Influence of cell wall thickness variations on elastic stiffness of closed cell cellular solids, to appear.

Grenestedt, J.L., Tanaka, K., 1998. Influence of cell shape variations on elastic stiffness of closed cell cellular solids, to appear.

Guo, X.E., Gibson, L.J., McMahon, T.A., Hayes, W.C., 1999. Post yield behaviour of intact and damaged honeycombs: A finite element study, Int. J. Mech. Sci., submitted.

Hodge, P.G., 1959. Plastic Analysis of Structures. McGraw-Hill, London.

Klintworth, J., Stronge, W., 1988. Elasto-plastic yield limits and deformation laws for transversely crushed honeycomb. Int. J. Mech. Sci. 30, 273–292.

Klintworth, J., Stronge, W., 1989. Plane punch indentation of a ductile honeycomb. Int. J. Mech. Sci. 31, 359–378.

Klocker, T. 1998 private communication.

Kraynik, A.M., Reinelt, D.A., Princen, H.M., 1991. The non-linear elastic behaviour of polydisperse hexagonal foams and concentrated emulsions. J. Rheol. 35, 1235–1253.

Kraynik, A.M., Neilsen, M.K., Reinelt, D.A., Warren, W.E., 1997. Foam micromechanics. In: Proceedings of the NATO Advanced Study Institute on 'Foams, Emulsions, and Cellular Materials', Cargese, Corsica.

Olurin, O.B., Fleck, N.A., Ashby, M.F., 1999. The mechanical properties of aluminium foams under uniaxial loading, Acta mater., submitted for publication.

Silva, M.J., Hayes, W.C., Gibson, L.J., 1995. The effect of non-periodic microstructure on the elastic properties of two-dimensional cellular solids. Int. J. Mech. Sci. 37, 1161–1177.

Silva, M.J., Gibson, L.J., 1997. The effect of non-periodic microstructure and defects on the compressive strength of two-dimensional cellular solids. Int. J. Mech. Sci. 39, 549–563.

Simone, A.E., Gibson, L.J., 1998a. The effect of solids distribution on the stiffness and strength of metallic foams. Acta mater. 46, 2139–2150.

Simone, A.E., Gibson, L.J., 1998b. The effects of cell face curvature and corrugations on the stiffness and strength of metallic foams. Acta mater. 46, 3929–3935.

Sugimura, Y., Meyer, J., He, M.Y., Bart-Smith, H., Grenestedt, J.L., Evans, A.G., 1997. On the mechanical performance of closed cell Al alloy foams. Acta mater. 45, 5345–5359.

Triantafyllidis, N., Schraad, M.W., 1998. Onset of failure in aluminium honeycombs under general in-plane loading. J. Mech. Phys. Solids 46, 1089–1124.

Warren, W.E., Kraynik, A.M., 1987. Foam mechanics: the linear elastic response of two-dimensional spatially periodic cellular materials. Mech. Mater. 6, 27–37.

Weaire, D., Kermode, J.P., Wejchert, J., 1986. On the distribution of cell area in a Voronoi network. Phil. Mag. B 53, L101–L105.

Weaire, D., Fortes, A.M., 1994. Stress and strain in liquid and solids foams. Advances in Physics 43, 685–738.